Open Journal of Chemistry

PSR Press

Article

Facile synthesis of Nickel-iron based electrocatalyst anodes for efficient oxygen evolution reaction

Aisha Batool[1,*], Farah Kanwal[2], Shahzad Ahmad[3], Sumreen Asim[4] and Murtaza Saleem[5]

1 School of Phyical Sciences, University of the Punjab, Lahore 54590, Pakistan.
2 Institute of Chemistry, University of the Punjab, Lahore-54590, Pakistan.
3 School of Economics and Management, Beijing Forestry University, Beijing-100083, China.
4 Khwaja Fareed University of Engineering and Information Technology, Department of Chemistry, 64200-RYK, Pakistan.
5 Department of Physics, Syed Babar Ali School of Science and Engineering, Lahore University of Management Sciences (LUMS), 54792-Lahore, Pakistan.
* Correspondence: dr.batool.aisha@gmail.com

Received: 18 May 2020; Accepted: 27 August 2020; Published: 7 November 2020.

Abstract: In this research, we reported facile synthesis of efficient Ni_3Fe electrocatalyst nanostructures deposited on conducting carbon fibers surface by a simple chemical bath deposition method at moderate temperature. The composition, phase and electrocatalytic property of as-prepared binder-free electrocatalyst was characterized by X-ray diffraction (XRD), field emission scanning electron microscopy (FE−SEM), and electrochemical measurements. The as−synthesized $Ni_3Fe@t-CF$ presented excellent performance and durability as water oxidation electrocatalyst in alkaline electrolyte owing to non−segregated deposition of Ni_3Fe nanostructures on conducting surface of carbon, high electrochemical surface area, and the fast absorption and desorption of water molecules during oxygen evolution reaction due to the $3D$ architecture of conducting interlaced carbon fibers template.

Keywords: Chemical deposition, Ni_3Fe nanostructures, carbon cloth fibers, electrochemical surface area, conductivity, oxygen evolution.

1. Introduction

Impeding global energy crises became the world extremely defensive over their natural resources and it is crucial to seek alternative energy conversion and storage systems such as water electrolysis, fuel cells and metal-air batteries [1]. Oxygen evolution reaction (OER) is bottleneck in water splitting and is process of generating molecular oxygen through electrochemical oxidation of water [2]. Nevertheless, OER process suffers from sluggish kinetics with a complicated multi-electron transfer step, resulting in a high overpotential requirement [3]. An effective electrocatalyst is needed in order to expedite the OER reaction to reduce the overpotential, and thus enhance energy conversion efficiency. Currently, noble metal oxides such as IrO_2 or RuO_2 are the benchmark water oxidation electrocatalysts in alkaline solutions, but their scarcity, high cost and poor stability restrict their implementation as water oxidation electrocatalyst at large scale [4–7]. In this regard, the exploit of earth-abundant, stable and highly efficient water oxidation electrocatalysts are highly needed.

A wide range of non-noble metal electrocatalysts have been developed with promising water oxidation performance including, transition-metal oxides, sulfides and nitrides [8–12]. Among these developed electrocatalysts, the nickel-iron based materials have attracted intensive attention because of their high water oxidation activity and stability [13]. However, they exclusively yield low catalytic activity owing to their insufficient intrinsic electrical conductivity and small surface area of the catalyst structures. Recently, combining highly conductive scaffold materials with inexpensive transition metal oxides have been used to enhance charge transport properties; thereby promoting catalytic activity. However, most of these fabricated materials exhibit buried active sites due to segregated morphology. Expensive synthetic protocols have been adopted to address these problems [14–16].

Herein, we report a simple strategy to develop binder-free nickel-iron based electrocatalyst films by adopting chemical bath deposition technique at moderate temperature. The developed Ni_3Fe nanostructures deposited on carbon scaffold exhibited high OER performance with stability up to 6500s with the 89% activity

retention in alkaline electrolyte under vigorous bubbling across its electrode surface corresponding to $J = 10$ mA cm^{-2} (overpotential $=$ 320V versus RHE). This improvement in the OER performance correlated with the significantly improved conductivity and the large electrochemical active surface area to provide more accessible catalytic active sites for the adsorption and desorption of water oxidation intermediates. We believe that this would be an attractive and facile strategy for the cost-effective development of efficient nickel-iron based water oxidation catalyst.

2. Materials and Methods

Isopropyl alcohol (HPLC, $\geq$ 99.5%), ethanol (AR, $\geq$ 99.7%), iron nitrate $(Fe(NO_3)_3 9H_2O)$ (AR grade, 99.9%), nickel nitrate $(Ni(NO_3)_2 6H_2O)$ (99.9%, Aladdin Industrial Co., Ltd.) and KOH (AR grade, 99%) were used in this experimental work. Double distilled water was used in preparing solutions and washing of electrodes.

2.1. Synthesis of t-CF

The cut pieces of CF ($11cm^2$) were washed with isopropyl alchohol, ethanol and then water in succession, each for 5 minutes in water bath sonication and then oxidized by using previously reported modified Hummers method and named as $t-CF$ [17].

2.2. Synthesis of Ni3Fe@t-CF

Typically, the $Ni_3Fe@t-CF$ electrocatalyst was prepared by chemical bath deposition technique at room temperature. The deposition of Ni_3Fe nanostructures on $t-CF$ surface was carried out using chemical bath solution containing $Ni(NO_3)_2.6H_2O$ (3 mM) and $Fe(NO_3)_3.9H_2O$ (1 mM). The chemical bath solution was continuously purged with Ar gas during electrodeposition to avoid the oxidation of Fe^{2+} to Fe^{3+}. The deposition was carried by oil bath heating at 80^0C for 2 hours.

2.3. Characterizations

FE-SEM was carried out using a Hitachi *S*4800 with a 10kV accelerating voltage. XRD was performed on a PANanalytical XPert powder diffractometer at operating voltage of 40kV and operating current of 40mA. All electrochemical measurements were carried out in a 3-electrode cell in 1 M KOH electrolyte solution (pH $\sim$ 13.6) using CHI 760 electrochemical workstation. As-prepared $Ni_3Fe@t-CF$, t-CF and CF samples were used directly as the working electrodes. All measured potentials were calibrated to RHE using the following Equation (1);

$$E_{RHE} = E_{SCE} + 0.244V + 0.059 \times pH. \tag{1}$$

Linear sweep voltammetry (LSV) polarization and cyclic voltammetry (CV) curves in non-Faradaic potential region (0.10.2 V versus RHE) were recorded at a scan rate of 10 mVs^{-1}. Tafel slopes were derived from the corresponding OER polarization curves with iR compensation in alkaline solution for $Ni_3Fe@t-CF$, $t-CF$ and CF using following Equation (2);

$$\eta = a + blog(j), \tag{2}$$

where η is the overpotential, whose value can be calculated from Equation (3);

$$E(\eta) = E(SCE) + 0.244 + (0.059 \times pH)1.23, \tag{3}$$

where b is the Tafel slope measured in mV/dec and j is the current density. The chronoampermetric measurements were conducted under the same above described experimental conditions but without iR drop compensation.

The electrochemical active surface area (ECSA) of samples CF, $t-CF$ and $Ni_3Fe@t-CF$ were calculated from the electrochemical double layer capacitance (C_{dl}). The scan-rate (v) dependent capacitive current, I_c is associated with the C_{dl} according to relation:

$$ECSA = C_{dl} = I_c/v, \tag{4}$$

where $I_c = I_{anodic} I_{cathodic}$, calculated in the middle of potential domain as a function of scan rate v, that yielded a linear slope equal to $2 \times C_{dl}$.

Electrochemical impedance spectroscopy (EIS) was used to evaluate the electrochemical response of the synthesized OER electrocatalysts towards an applied alternating potential and to find the resistance in the transfer of charges (R_{CT}). The EIS measurements were conducted at 1.44 V versus RHE in the frequency range 100 kHz to 0.1 Hz with 10 mV amplitude of sinosoidal wave.

3. Results

3.1. X-ray Diffraction (XRD)

Phase determination of the CF, t-CF and $Ni_3Fe@t-CF$ was carried out by XRD analysis and their XRD patterns as shown in Figure 1. Figure 1(a) shows the graphite nature of CF and t-CF (JCPDS card no. $03-1185$). While the characteristic diffraction peaks of graphite at 25.6^0 and 43^0 are less intense in t-CF in comparison to CF, demonstrates its less ordered crystalline structure. Figure 1(b) shows the intense diffraction peaks at 44.9^0, 52.39^0 and 76.73^0 that correspond to (111), (200) and (220) planes of crystalline Ni_3Fe and matches with JCPDS card no. $48-0419$.

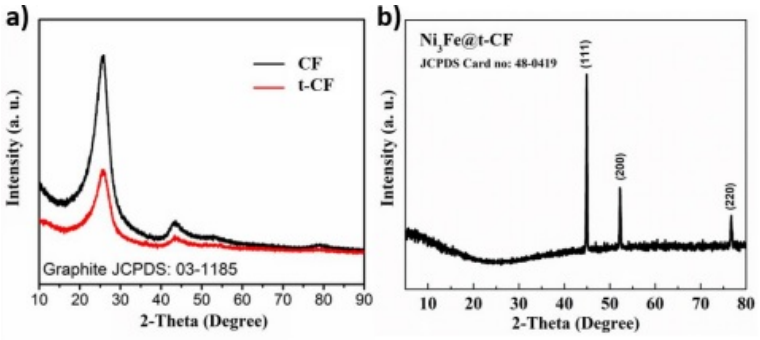

Figure 1. XRD patterns of (a) CF and t-CF and (b) $Ni_3Fe@t-CF$.

3.2. Field-Emission Scanning Electron Microscope (FE-SEM)

Figure 2(a) shows the FE-SEM image of pristine CF containing 3-dimensional framework of interlaced carbon fibers with void spaces between them. The high magnification image of the red squared area in Figure 2(a) shows the smooth surface of the CF. While the Figure 2(d) shows the high magnification image of the red squared area in Figure 2(c) that presents the dispersion of highly porous nickel-iron alloy nanostructures with high surface area on the smooth surface of CF. The high surface area with more exposed active sites, electrolyte penetration and fast adsorption and desorption of the generated gas bubbles facilitate OER activity.

3.3. Linear Sweep Voltammetry (LSV)

The LSV polarization curves of pristine CF, $t-CF$ and $Ni_3Fe@t-CF$ are shown in Figure 3. The OER performance was evaluated from onset and the overpotentials needed to drive current density of 10 mAcm^{-2} measured from corresponding LSV curves in alkaline electrolyte using standard 3-electrode electrochemical system. The pristine CF, $t-CF$ and $Ni_3Fe@t-CF$ exhibit the onset potentials of $1.6, 1.57$ and 1.48 V versus RHE, respectively. The significantly lower overpotenial needed for 10 mAcm^{-2} was 320 V for $Ni_3Fe@t-CF$. While both pristine CF and $t-CF$ exhibit negligible OER activity with very small current densities of 2 mAcm^{-2} and 1.7 mAcm^{-2}, respectively at 1.7 V versus RHE. The large surface area is resulting from the highly porous and rough surface of $Ni_3Fe@t-CF$ electrocatalyst as evident in its SEM images. While the efficient intrinsic OER activity is owing to more exposed active sites for the OER reactants.

3.4. Tafel Slope

The Tafel plots for all the materials were generated from the LSV polarization curves by plotting the log of current $(\log I)$ against the applied potentials (V_{SCE}). The Tafel slopes (b) were extracted by fitting straight line portion of the Tafel plots to the Tafel equation (Equation (2)). Figure 4 shows the Tafel slopes of CF, $t-CF$ and $Ni_3Fe@t-CF$ derived from their respective LSV polarization curves to show the influence of the applied

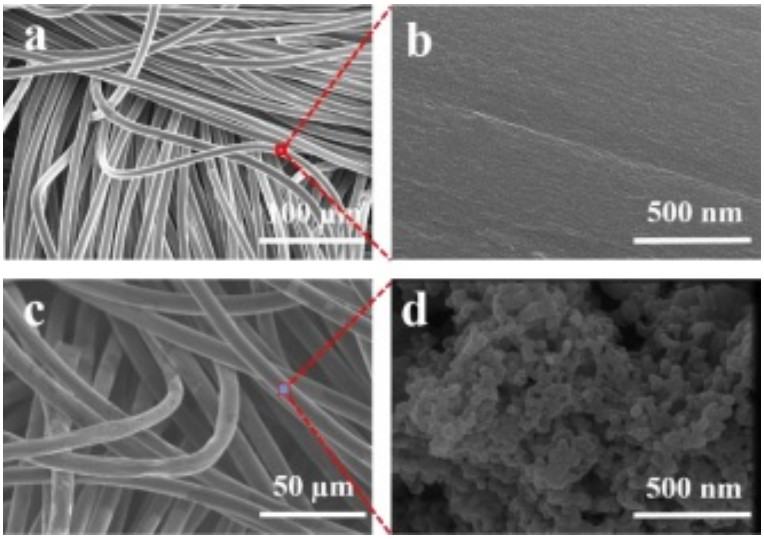

Figure 2. SEM image of (a) pristine CF, (b) high resolution SEM image of the area squared in (a), (c) $Ni_3Fe@t-CF$ and (d) high resolution SEM image of the area squared in (c).

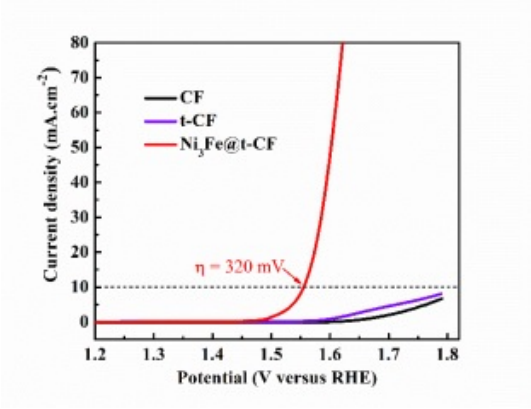

Figure 3. LSV curves (with iR correction) of CF (black curve), $t-CF$ (purple curve) and $Ni_3Fe@t-CF$ (red curve) in alkaline electrolyte.

OER overpotential on the current density (I) to evaluate their OER kinetics. The Tafel slope for $Ni_3Fe@t-CF$ was about 65 mV/dec that is comparable to the previously reported nickel-iron based electrocatalysts [17].

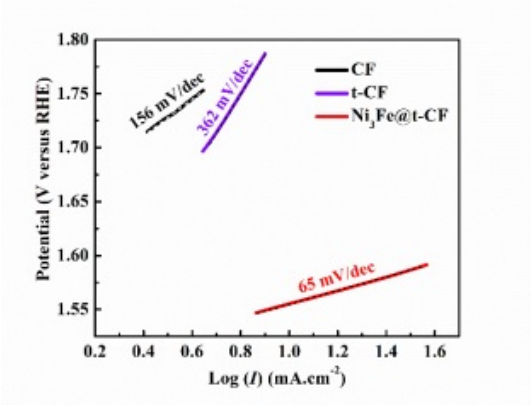

Figure 4. Tafel slopes of CF (black curve), $t-CF$ (purple curve) and $Ni_3Fe@t-CF$ (red curve) in alkaline electrolyte.

3.5. Electrochemical active surface area (ECSA) measurements

Figure 4(a-c) show the CV curves for pristine CF, $t-CF$ and $Ni_3Fe@t-CF$ in the non-Faradaic potential region from 0.1 to 0.2V in alkaline solution. Where for these CV measurements, CV curves were run at multiple scan rates (v) of $20, 40, 60, 80, 100, 150, 200, 250, 300$ and $350 mVs^{-1}$. The plot of capacitive current (I_c) at the middle of the applied potential window versus v gives C_{dl} that has direct relation with ECSA as given in equation (4). Figure 5(d) shows that $Ni_3Fe@t-CF$ exhibits the highest ECSA of $1.7 mFcm^{-2}$ in comparison to $t-CF$ $(0.87 mFcm^{-2})$ and $CF(0.44 mFcm^{-2})$. The larger ECSA is resulting from the highly porous and rough surface of $Ni_3Fe@t-CF$ as evident in its SEM images. The efficient intrinsic OER activity is owing to more accessible active sites of this electrocatalyst for the reactant species.

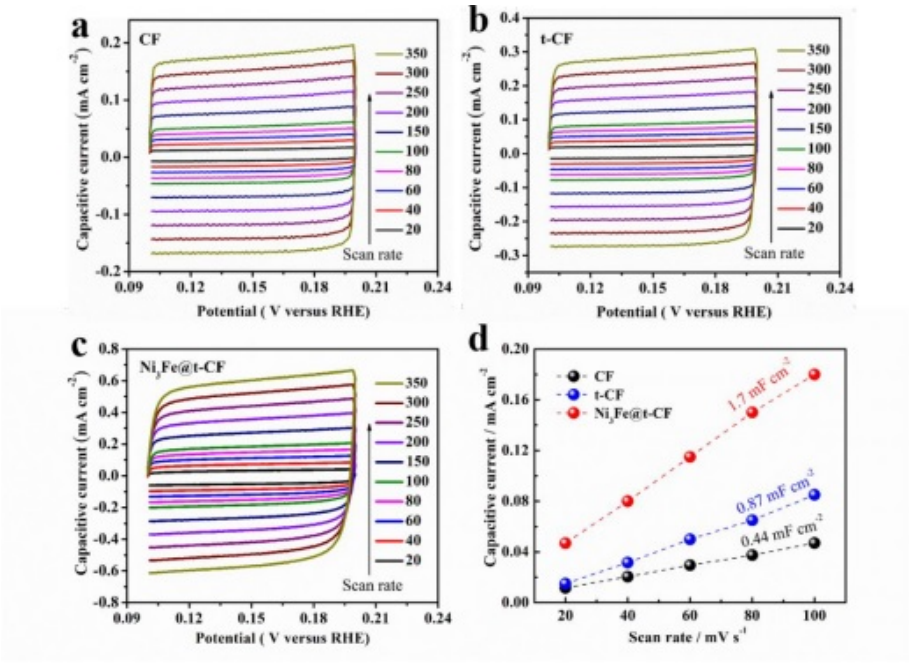

Figure 5. CV curves in non-Faradaic region (a) CF, (b) $t-CF$ and $Ni_3Fe@t-CF$. (d) Calculated C_{dl} plots of CF (black curve), $t-CF$ (blue line) and $Ni_3Fe@t-CF$ (red line).

3.6. Electrochemical Impedance Spectroscopy (EIS)

Further, electrochemical impedance spectroscopy (EIS) measurements were carried out to study the kinetics of interfacial electrocatalytic behaviour of CF, $t-CF$ and $Ni_3Fe@t-CF$. The obtained Nyquist plots and charge transfer resistances (R_{CT}) are shown in the Figure 6. These plots showing two semicircles corresponding to RCT at the electrocatalyst/electrolyte interface and in the electrocatalyst electrode, in the low and high frequency regions, respectively. The semicircle for the $Ni_3Fe@t-CF$ in the high frequency range indicates the enhanced charge transport with very less R_{CT} 0.9ω in comparison to CF and $t-CF$. It reveals the good conductivity and the good interfacial contact between the $3D$ conducting framework of CF and the Ni_3Fe electrocatalyst.

3.7. Chronoamperometric Measurements

Durability is an important feature to evaluate OER activity for practical applications at large scale. The stability of the as-synthesized $Ni_3Fe@t-CF$ electrocatalyst was recorded over $6500s$ in alkaline electrolyte at $1.54V$ versus RHE (without iR drop compensation). Figure 7 shows good stability of $Ni_3Fe@t-CF$ electrocatalyst by preserving a relative 89% of the initial current density of $10 mAcm^{-2}$ suggesting its good operational stability in the alkaline solution.

4. Conclusion

In this work, we have used a facile and effective strategy for the synthesis of Ni_3Fe nanostructures deposited on the $3D$ conducting surface of carbon at moderate temperature as an efficient OER catalyst in alkaline electrolyte. The high OER performance of the as-synthesized $Ni_3Fe@t-CF$ sample is attributed to

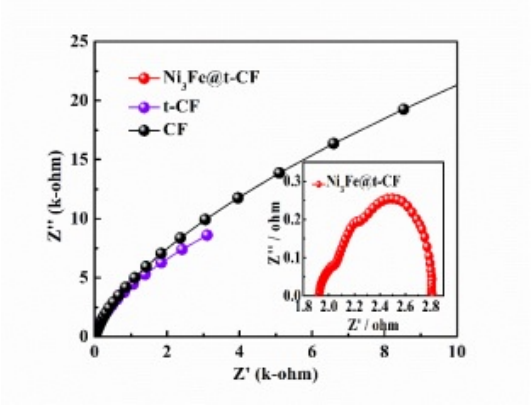

Figure 6. Nyquist plots of of CF (black curve), $t-CF$ (purple curve) and $Ni_3Fe@t-CF$ (red curve) in alkaline electrolyte.

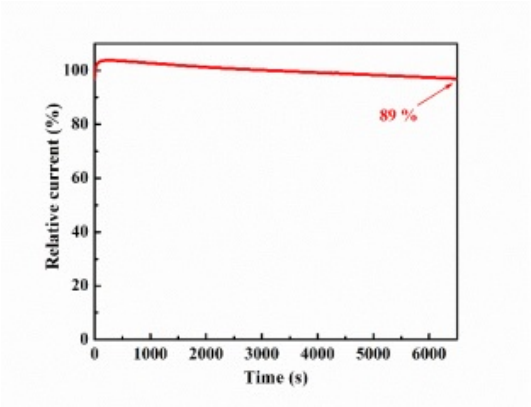

Figure 7. Chronoamperometric test of $Ni_3Fe@t-CF$ at 1.54 V versus RHE.

the high electrochemical active surface area as inferred from its FE-SEM images, low charge transfer resistance due to intimate contact between electrocatalyst nanostructures and the $3D$ conducing template. Considering the high performance of our synthesized binder-free electrocatalyst, this work will undeniably provide a prospect for the development of inexpensive and highly active OER electrocatalyst films by adopting this simple synthetic technique.

Acknowledgments: The authors gratefully acknowledge financial support provided by the Higher Education Commission (HEC), Islamabad. Special gratitude to School of Physical Sciences, the Institute of Chemistry, University of the Punjab and LUMS Pakistan for conducting experimental work and electrochemical measurements. This research work is financially supported by the Higher Education Commission (HEC) of Pakistan under the program (IPFP/HRD/HEC/20192352).

Author Contributions: A.B. designed and perform the experimental work and participated in data compilation and interpretation F. K. participated in data analysis and drafted the manuscript. All authors drafted the manuscript and gave final approval to publish this article.

Conflicts of Interest: "The authors declare no conflict of interest."

References

[1] Abe, J. O., Popoola, A. P. I., Ajenifuja, E., & Popoola, O. M. (2019). Hydrogen energy, economy and storage: review and recommendation. *International Journal of Hydrogen Energy, 44*(29), 15072–15086.

[2] Zhao, Y., Nakamura, R., Kamiya, K., Nakanishi, S., & Hashimoto, K. (2013). Nitrogen-doped carbon nanomaterials as non-metal electrocatalysts for water oxidation. *Nature Communications, 4*(1), 1–7.

[3] Walter, M. G., Warren, E. L., McKone, J. R., Boettcher, S. W., Mi, Q., Santori, E. A., & Lewis, N. S. (2010). Solar water splitting cells. *Chemical Reviews, 110*(11), 6446–6473.

[4] Sun, Y., Delucchi, M., & Ogden, J. (2011). The impact of widespread deployment of fuel cell vehicles on platinum demand and price. *International Journal of Hydrogen Energy, 36*(17), 11116–11127.

[5] Risch, M., Stoerzinger, K. A., Maruyama, S., Hong, W. T., Takeuchi, I., & Shao-Horn, Y. (2014). $La_{0.8}Sr_{0.2}MnO_{3-\delta}$ decorated with $Ba_{0.5}Sr_{0.5}Co_{0.8}Fe_{0.2}O_{3-\delta}$: a bifunctional surface for oxygen electrocatalysis with enhanced stability and activity. *Journal of the American Chemical Society, 136*(14), 5229–5232.

[6] Li, Y., Gong, M., Liang, Y., Feng, J., Kim, J. E., Wang, H., ... & Dai, H. (2013). Advanced zinc-air batteries based on high-performance hybrid electrocatalysts. *Nature communications, 4*(1), 1–7.

[7] McCalla, E., Abakumov, A. M., Saubanère, M., Foix, D., Berg, E. J., Rousse, G., ... & Dominko, R. (2015). Visualization of O-O peroxo-like dimers in high-capacity layered oxides for Li-ion batteries. *Journal of Science, 350*(6267), 1516–1521.

[8] Zhou, D., Cai, Z., Lei, X., Tian, W., Bi, Y., Jia, Y., ... & Pan, J. (2018). NiCoFe-Layered Double Hydroxides/N-Doped Graphene Oxide Array Colloid Composite as an Efficient Bifunctional Catalyst for Oxygen Electrocatalytic Reactions. *Advanced Energy Materials, 8*(9), 1701905.

[9] Li, T., Lv, Y., Su, J., Wang, Y., Yang, Q., Zhang, Y., ... & Tang, Y. (2017). Anchoring $CoFe_2O_4$ nanoparticles on N-doped carbon nanofibers for high-performance oxygen evolution reaction. *Advanced Science, 4*(11), 1700226.

[10] McCrory, C. C., Jung, S., Ferrer, I. M., Chatman, S. M., Peters, J. C., & Jaramillo, T. F. (2015). Benchmarking hydrogen evolving reaction and oxygen evolving reaction electrocatalysts for solar water splitting devices. *Journal of the American Chemical Society, 137*(13), 4347–4357.

[11] Li, B. Q., Xia, Z. J., Zhang, B., Tang, C., Wang, H. F., & Zhang, Q. (2017). Regulating p-block metals in perovskite nanodots for efficient electrocatalytic water oxidation. *Nature Communications, 8*(1), 1–7.

[12] Ling, T., Yan, D. Y., Wang, H., Jiao, Y., Hu, Z., Zheng, Y., ... & Jaroniec, M. (2017). Activating cobalt (II) oxide nanorods for efficient electrocatalysis by strain engineering. *Nature Communications, 8*(1), 1–7.

[13] Yu, L., Zhou, H., Sun, J., Qin, F., Yu, F., Bao, J., ... & Ren, Z. (2017). Cu nanowires shelled with NiFe layered double hydroxide nanosheets as bifunctional electrocatalysts for overall water splitting. *Energy & Environmental Science, 10*(8), 1820–1827.

[14] Ye, Z., Li, T., Ma, G., Dong, Y., & Zhou, X. (2017). Metal-Ion (Fe, V, Co, and Ni)-doped MnO_2 ultrathin nanosheets supported on Carbon fiber paper for the oxygen evolution reaction. *Advanced Functional Materials, 27*(44), 1704083.

[15] Zhang, B., Zheng, X., Voznyy, O., Comin, R., Bajdich, M., García-Melchor, M., ... & de Arquer, F. P. G. (2016). Homogeneously dispersed multimetal oxygen-evolving catalysts. *Journal of Science, 352*(6283), 333–337.

[16] Lv, Y., Batool, A., Wei, Y., Xin, Q., Boddula, R., Jan, S. U., ... & Gong, J. R. (2019). Homogeneously distributed NiFe alloy nanoparticles on 3D carbon fiber network as a bifunctional electrocatalyst for overall water splitting. *ChemElectroChem, 6*(9), 2497–2502.

[17] Sakita, A. M. P., Valles, E., Della Noce, R., & Benedetti, A. V. (2018). Novel NiFe/NiFe-LDH composites as competitive catalysts for clean energy purposes. *Applied Surface Science, 447*, 107–116.

[18] Jadhav, H. S., Roy, A., Desalegan, B. Z., & Seo, J. G. (2020). An advanced and highly efficient Ce assisted NiFe-LDH electrocatalyst for overall water splitting. *Sustainable Energy & Fuels, 4*(1), 312–323.